Hydrogen production from the catalytic dehydrogenation of dodecahydro-N-ethylcarbazole : effect of Pd precursor on the catalytic performance of Pd/C catalysts

Zhaolu Feng
Harbin Engineering University
Xiaomin Chen
Institute of petrochemical, Heilongjiang Academy of sciences
Xuefeng Bai (tommybai@126.com)
Institute of Petrochemical, Heilongjiang Academy of Sciences https://orcid.org/0000-0002-8757-7034

Research Article

Keywords: Hydrogen production, Liquid organic hydrogen carrier, Dodecahydro-N-ethylcarbazole, Pd precursor, glow-discharge plasma

Posted Date: May 4th, 2021

DOI: https://doi.org/10.21203/rs.3.rs-404448/v1

Abstract

In this paper, Pd/C catalysts are synthesized via Ar glow-discharge plasma reduction using activated carbon as the support and $Pd(acac)_2$, $Pd(NO_3)_2$, K_2PdCl_4 and H_2PdCl_4 as the Pd precursors, and their catalytic performance are investigated by hydrogen production from dodecahydro-N-ethylcarbazole (H12-NEC). Pd/C-A, prepared from $Pd(acac)_2$, with the smallest palladium nanoparticles (1.7 nm), the highest dispersion (34%) and no residue of inorganic ions exhibits the best catalytic activity with a hydrogen release of 5.28 wt.%, which is 2.2 times that of Pd/C-H. The order of the apparent activation energies of as-prepared Pd/C catalysts from the kinetics of H12-NEC dehydrogenation reaction as follows: Pd/C-A ≈ Pd/C-N□Pd/C-K□Pd/C-H. For $Pd(acac)_2$ with a large ligand, as a cation Pd precursor, the effect of Coulomb attraction to Pd^{2+} during the plasma reduction process makes it difficult for Pd nanoparticles (NPs) to migrate, which leads to the formation of ultrafine Pd NPs.

1. Introduction

Hydrogen, the lightest elements in the periodic table, is found to be easily produced by electrolysis and photoelectrolysis of water, hydrocarbon reforming and biological processes. It is important new energy due to its possess great merits, such as high heating value per mass, regenerative, non-toxic, environmentally friendly, and so on (Das and Veziroğlu 2001; Holladay et al. 2009; Modisha et al. 2019; Veziroğlu and Şahi ̇n 2008; Zhang et al. 2016). However, so far hydrogen energy cannot be applied on a large scale due to its inability to be stored and transported efficiently (Moradi and Groth 2019). Liquid organic hydrogen carrier (LOHC), a pair of organic compounds with high boiling points, is proposed to store hydrogen via highly reversible hydrogenation and dehydrogenation reactions (Gianotti et al. 2018; Preuster et al. 2017; Wulf and Zapp 2018). The LOHC-based technology has been indeed considered safe and convenient solutions for hydrogen storage and has the potential to fulfill the demands of mobile devices, especially automotive applications (Aakko-Saksa et al. 2018; Crabtree 2017; He et al. 2016). Among the hydrogen storage cycle in LOHC systems, the hydrogenation process can be done in a factory and reaction conditions are easy to be satisfied because its thermodynamically favorable, and Ru catalysts have exhibited excellent catalytic performance. On the contrary, providing hydrogen, that is, the dehydrogenation process is often used in a variety of mobile devices, which makes it face some bottleneck problems, so the research for LOHC dehydrogenation was emphasized. (Eblagon et al. 2010; Eblagon et al. 2012; Sotoodeh and Smith 2013).

Among numerous organic materials, the hydrogen storage density of LOHC candidate compounds must meet a target of no less than 5.5 wt.% as promulgated by the U.S. Department of Energy for 2020, boiling points above 200°C and melting points below − 40°C (Satyapal et al. 2007). In early times, some cycloalkanes compounds, such as naphthalene and cyclohexane, were chosen as LOHC, but it was found that dehydrogenation of these compounds required high temperature to maintain the catalyst activity and resulting in the generation of a massive by-product because of the breakage of the C-C bond, which would negatively influence the practical application of LOHC system (Aramendía et al. 1997; Hodoshima

et al. 2003; Makowski et al. 2009). Recent studies on LOHC dehydrogenation have demonstrated that the aromatic hydrocarbons with N-heterocycle such as N-ethylcarbazole (NEC), 2-(n-methylbenzyl) pyridine, 2-methylpiperidine, can significantly reduce the dehydrogenation temperature and increase the H_2 recovery rate, which indicates that there were more suitable for hydrogen storage (Oh et al. 2018; Sobota et al. 2011; Xie and Milstein 2019). Up to now, many LOHC systems have been successfully developed. In spite of that, because of its high hydrogen storage ability (5.79 wt%), NEC, as the earliest proposed LOHC, is regarded as the most promising candidate for hydrogen storage and its low enthalpy of dehydrogenation (Papp et al. 2014; Stark et al. 2015; Zhu et al. 2018). Complete dehydrogenation of dodecahydro-N-ethylcarbazole (H12-NEC) that is the full hydrogenation product of NEC can be achieved below 200 ℃ (Yang et al. 2012). Compared with dodecahydrocarbazole and dodecahydrofluorene, the highest catalytic activity for H12-NEC dehydrogenation was found owing to the ethyl group in H12-NEC prevented a strong interaction between the catalyst and the N atom (Sotoodeh et al. 2012). However, H12-NEC dehydrogenation faces many challenges,which leads to a certain distance to go to achieve the practical application of the NEC/H12-NEC hydrogen storage. Based on the previous research results, we still need to continue to do a lot of work to further accelerate the reaction rate, reduce the reaction temperature. The key point of the research is to find catalysts with excellent dehydrogenation performance.

At present, the dehydrogenation catalysts on studying can divide into two kinds: heterogeneous and homogeneous catalysts (Fei et al. 2017; Peters et al. 2015; Tarasov et al. 2018; Wang et al. 2009). Although the homogeneous catalysts have high catalytic activity, the difficult separation and recycle of the catalysts also limit their application (Wang et al. 2019b). Supported metal nanoparticles (NPs) catalysts, as heterogeneous catalysts, have attracted intense attention because it shows outstanding catalytic performance in various dehydrogenation reactions. Pd-based and Pt-based catalysts are extensively studied and therefore the dehydrogenation mechanism of H12-NEC on these catalysts is comparatively clear (Amende et al. 2014a; Amende et al. 2014b; Kim et al. 2021; Wang et al. 2020; Wang et al. 2017). Previous studies had found that both Pd and Pt catalysts can significantly enhance the dehydrogenation performance of H12-NEC compared with commercial catalysts but there were still some gaps for them in terms of catalytic efficiency (Kim et al. 2017). Yang (Yang et al. 2014) investigated H12-NEC dehydrogenation over Pd, Pt, Ru and Rh catalysts supported on Al_2O_3 and indicated that the initial catalytic activity of Pd was better than other catalysts. There are many materials used as dehydrogenation catalyst supports, such as carbon including its allotropes, Al_2O_3, SiO_2 and so on. Because of the various physicochemical properties of the support, the catalytic performance was very different. Activated carbon is one of the simple, common and low-cost supports, with it as a support to show high activity in dehydrogenation reaction. Xie and Milstein (Xie and Milstein 2019) prepared Pd catalysts using different supports including activated carbon, SiO_2, γ-Al_2O_3, CeO_2 and boron nitrile. The results of 2-methylpiperidine dehydrogenation showed that Pd/C was the most effective catalyst with the conversion of 98% and hydrogen yield of 91% at 170 ℃. Cui (Cui et al. 2008) studied the effect of support on 4-aminopiperidine dehydrogenation performance over Pd-based catalysts to find that the Pd/C exhibited the highest catalytic activity.

A critical step in the preparation of supported metal catalysts is the reduction process of metal ions. The hydrogen reduction was carried out at the higher temperatures, which was not beneficial to the distribution of metals due to serious aggregations. The chemicals used in the reduction process can bring many environmental problems, which is not consistent with green chemistry principals (Deng et al. 1999; Mallick et al. 2004; Schmidt 2001). Kim (Kim and Kim 2019) prepared Pd/C catalysts using $NaBH_4$ reduction. It was observed that the Pd particles were typically agglomerated from 2.5 nm to 4.8 nm with an increase of $NaBH_4$, which resulted in a decrease in catalytic activity for formic acid dehydrogenation reaction. Recently, alternative reduction technology has attracted much attention. Plasma is the fourth state of a substance that is different from solids, liquids and gases, consisting of molecules, neutral species, electrons, activated atoms and ions, which are excellent reducing agents (Zhang et al. 2018). The use of glow discharge plasma for the preparation of supported metal nanoparticles can be accomplished at near room temperature and without the addition of harmful reducing and stabilizing agents to avoid metal nanoparticle agglomeration, which can obtain high dispersion and metal utilization efficiency catalyst. This method is an in-situ, environmentally-friendly and straightforward technique (Liu et al. 2014; Liu et al. 2018; Xu et al. 2015). Liu (Liu and Bai 2016) prepared Pd nanoparticles (NPs) using N_2 glow discharge plasma reduction method. It was found that the smaller particle size and higher dispersion of Pd NPs were obtained compared to L-ascorbic acid reduction method, and thereby improving catalytic performance for Suzuki coupling reaction. Liu (Liu et al. 2019) successfully prepared Pd NPs supported on N-doped reduced graphene oxide (Pd/PNGO) catalyst via N_2 glow discharge plasma reduction method. Pd/PNGO for the reduction of 4-nitrophenol has higher activity (TOF of 366.9 h^{-1}). Zou (Zou et al. 2006) synthesized Pd, Pt, Ag and Ag NPs supported on TiO_2 and Al_2O_3 by argon glow discharge plasma. They found that all metal ions were completely reduced within 60 minutes and the degree of reduction gradually increases with the prolonging of treatment time. Among these catalysts, Pd had the smallest particle size of 2.1 nm. Di (Di et al. 2019) successfully prepared the Pd/C catalyst (Pd/C-P) by dielectric barrier discharge cold plasma. Compared with the commercial Pd/C, Pd/C-P had the better catalytic performance for the dehydrogenation reaction of formic acid. The total amount of gas generated on Pd/C-P and commercial Pd/C was 317 ml and 212 ml, respectively. Zhang (Zhang et al. 2020) synthesized PdAu/C-P by an atmospheric pressure cold plasma reduction method, and its formic acid dehydrogenation reactions were carried out. The results revealed that PdAu/C-P exhibited a better catalytic performance than PdAu/C-C which was reduced by hydrogen at 300 ℃ for 2 h. This was mainly due to the small particle size of PdAu/C-P and evenly distribution. Plasma provides a simple, environmentally-friendly and effective approach for the preparation of various sizes, structures, active sites and defects of supported metal catalysts.

For supported catalysts, the precursor is deemed to be one of the crucial factors for the nature of metal, which would have a direct effect on catalytic performance (Baylet et al. 2008; Kinnunen et al. 2009; Rotunno et al. 2006; Scirè et al. 2002). Li (Li et al. 2013; Xie et al. 2015) prepared Pd/SiO_2 catalyst using palladium(II) acetylacetonate ($Pd(acac)_2$), $Pd(NO_3)_2$ and $(NH_4)_2PdCl_4$ as precursors by impregnation method. The catalysts synthesized by $Pd(acac)_2$ exhibited excellent catalytic performance and anti-

sintering for the oxidation of methane due to its highly dispersed Pd particles. They found that the (≡ SiO_s)$_2$Pd intermediate was formed through hydrogen bond between the Pd(acac)$_2$ molecules and the silanol groups, and acacH species appeared after it was reduced, which plays a key role in promoting Pd particle dispersion. Panpranot (Panpranot et al. 2005) investigated hydrogenation of 1-hexene over Pd-based catalysts prepared respectively from $PdCl_2$, Pd(OOCCH_3)$_2$, and Pd(NO_3)$_2$. The results revealed that the silica-supported Pd catalysts using $PdCl_2$ as a precursor showed the best metal sintering properties. This was because the Pd particle size of these catalysts prepared by different precursors was different. Wang (Wang et al. 2015) used Pt(NO_3)$_2$, H_2PtCl_6, and Pt(NH_3)$_4Cl_2$ as precursors to prepare ZSM-22 zeolite loaded Pt-based catalysts, which was named 0.5P1, 0.5P2, and 0.5P3, respectively. The n-hexadecane hydroisomerization activities of these catalysts can be ranked as 0.5P2 > 0.5P1 > 0.5P3. They indicated that three factors affected the particle size and crystal structure of Pt, that is, the existence of chloride ions in the precursor, the location and the initial valence state of Pt. The structure and dispersion of metal particles are extremely dependent on the type of precursor. It is a valuable research issue for supported metal catalyst prepared from different precursors by plasma reduction.

Generally, Pd/C catalysts are suitable for H12-NEC dehydrogenation. The catalytic performance of the supported catalysts was strongly associated with the precursor and reduction method in the preparation process. Compared with traditional reduction methods, glow discharge plasma reduction was easier to obtain a catalyst with high dispersion, long thermal stability and good catalytic performance. Here, we employed the argon glow discharge plasma reduction method for the preparation of Pd/C using different precursors. The physicochemical properties of the catalysts were studied using a series of characterization techniques and H12-NEC dehydrogenation reaction was chosen as a model reaction to evaluate the catalytic performance.

2. Experimental

2.1 Materials

All reagents are used directly after purchase: Palladium chloride ($PdCl_2$, AR, Sinopharm Chemical ReagentCo., Ltd), Palladium acetylacetonate (Pd(acac)$_2$, AR, Zhejiang Metallurgical Research Institute Co.), Palladium nitrate (Pd(NO_3)$_2$·2H_2O, 39.5 wt.%Pd, Xi'an Kaili Catalyst New Materials CO., LTD), Hydrochloric acid (HCl, AR) and potassium chloride (KCl, AR) (Tianjin Tianli Chemical Reagent Co.), Activated carbon (AC, WENZHOU FAVORED TRADING CO., LTD), 5 wt.% Ru/Al_2O_3 (Alfa-Aesar), N-ethylcarbazole ($C_{14}H_{13}N$, AR, Tianjin Guangfu Fine Chemical Co., Ltd), argon (99.99%, Harbin Qinghua Industrial Gases Co.).

2.2 Synthesis of Pd/C Catalysts

The Pd/C catalysts were prepared via a simple wet impregnation route followed by Ar glow discharge plasma reduction method, and the loading amount of Pd was 5 wt.%. Aqueous H_2PdCl_4 and K_2PdCl_4 solution (0.01 mol/L) were prepared by mixing $PdCl_2$ with HCl and KCl in stoichiometric ratios. The

aqueous $Pd(NO_3)_2$ solution and $Pd(acac)_2$ toluene solution (0.01 mol/L) were prepared. 0.1 g AC and Pd precursor solution was added to 20 ml of deionized water and stirred for 12 h, then centrifuged, dried at 80°C (120°C for $Pd(acac)_2$) for 12 h. Then the obtained intermediate samples were reduced to Pd/C catalysts by argon glow discharge plasma under the conditions of system pressure of 70 Pa, discharge voltage of 2.1 A and reaction time of 90 min. The Pd/C catalysts prepared using $Pd(acac)_2$, $Pd(NO_3)_2$, K_2PdCl_4 and H_2PdCl_4 were denoted as Pd/C-A, Pd/C-N, Pd/C-K and Pd/C-H, respectively, and the above catalysts are hereafter collectively referred to as Pd/C catalysts.

2.3 Dehydrogenation of dodecahydro-N-ethylcarbazole

A detailed description of the H12-NEC dehydrogenation can be found in our previous work (Feng et al. 2020). H12-NEC (prepared by NEC, see the supporting information) and Pd/C catalysts were mixed in a three-necked flask for the reaction, and the molar ratio of Pd to H12-NEC was 0.03%. All reactions were performed at 180°C and 101 KPa unless otherwise mentioned. The diagram of the dehydrogenation reactor was shown in Fig. S2.

2.4 Catalyst Characterization

X-ray diffraction (XRD), X-ray photoelectron spectroscopy (XPS), N_2 adsorption/desorption, H_2 chemisorption, Thermogravimetric (TG) analysis, Zeta potentials analysis and high-resolution transmission electron microscopy (TEM) were used to characterize the structure, composition and morphology of activated carbon and the prepared Pd/C catalysts, with detailed test methods described in the supporting information

3 Results And Discussion

3.1 XRD

Figure 1 displayed the XRD pattern of the prepared Pd/C catalysts. All catalysts showed broad peaks at 21.6° corresponding to amorphous carbon, and a peak was found at 44.3° that can be assigned to the C(111) (JCPDS No. 80 – 0017), which may be stem from the slight graphitization of the activated carbon used itself. For Pd/C-N, Pd/C-K and Pd/C-H, the diffraction peaks at 40.2°, 46.8°, 68.3° and 82.4 were derived from the Pd (111), Pd (200), Pd (220) and Pd (311) (JCPDS No. 87–0641), which belonged to the face-centered cubic structure. Compared with other catalysts, no Pd peak was observed in Pd/C-A, which may be attributed to its smaller particle size and higher dispersion (Li et al. 2014). For Pd/C-K, the characteristic diffraction peaks of KCl (JCPDS NO. 75–0296) appear at 28.3°, 40.5° and 50.1° corresponding to KCl(200), KCl(220) and KCl(222), indicating KCl was formed during the reduction of K_2PdCl_4 using Ar glow discharge plasma.

3.2 XPS

The surface chemical composition of the prepared Pd/C catalysts and the chemical valences of Pd were analyzed by XPS. It can be seen from the full XPS spectra (Fig. S3) that C, Pd, and O were common elements for all samples, where Pd had two atomic orbitals, Pd 3d and Pd 3p. O elements may have

originated from the testing process as well as from the surface adsorption of O and H_2O. The peak of N 1s at 398.4 eV in Pd/C-N came from NO_3^- in $Pd(NO_3)_2$. Cl 2p and K 3p at 198.7 eV and 16.0 eV in Pd/C-K were derived from KCl produced by the decomposition of K_2PdCl_4, which was consistent with the XRD results. Similarly, the peak corresponding to Cl 2p also appeared in Pd/C-H, which may be derived from residual Cl after H_2PdCl_4 was reduced by Ar glow-discharge plasma. Table 1 showed that the atomic percentage of Cl (3.99%) of Pd/C-H was slightly higher than that of Pd/C-K (3.89%). Two spin-orbit splitting peaks Pd $3d_{3/2}$ and Pd $3d_{5/2}$ of Pd can be observed from Fig. 2. at 341.06 eV and 335.76 eV, which can be well fitted with two Pd^0 and two Pd^{2+} isolated peaks. These results suggest that the Pd^{2+} could partially originate from the unreduced Pd precursor and light oxidation during testing and their corresponding binding energy data were shown in Table 1. The peaks at 335.8 eV and 341.2 eV correspond to Pd^0 of Pd $3d_{5/2}$ and Pd $3d_{3/2}$, and the peak at 337.1 eV and 342.4 eV correspond to Pd $3d_{5/2}$ and Pd $3d_{3/2}$ Pd^{2+}. There was no significant difference in the peak positions of Pd^0 and Pd^{2+}, which indicated that the Ar gas glow discharge plasma was able to reduce the selected Pd precursor without affecting the valence of Pd. The reduction degree of Pd/C was determined from the peak areas of Pd^0 and Pd^{2+} and was listed in Table 1. The order of reduction degree was Pd/C-N > Pd/C-K > Pd/C-H > Pd/C-A. The standard electrode potentials of Pd^{2+}/Pd^0 and $[PdCl_4]^{2-}/Pd^0$ were 0.951 V and 0.591 V, indicating that $Pd(NO_3)_2$ was more easily reduced to Pd^0 than K_2PdCl_4 and H_2PdCl_4 under the same reducing conditions, so the reduction degree of Pd/C-N was the highest. As reported in previous studies (Yoshii et al. 2015), $Pd(acac)_2$ with the lower electrode potential and the greater coordination capacity of acetylacetonide compared to the halide-based anionic ligand, making it the most difficult to be reduced to Pd^0 and therefore the lowest reduction degree of Pd/C-A.

Table 1
XPS results of Pd/C catalysts

Catalysts	Pd $3d_{5/2}$ Binding Energy (eV)		Pd $3d_{3/2}$ Binding Energy (eV)		Degree of Reduction (%)	Cl atomic (%)
	Pd^0	Pd^{2+}	Pd^0	Pd^{2+}		
Pd/C-A	335.9	337.1	341.2	342.4	52.3	—
Pd/C-N	335.8	337.1	341.1	342.4	78.7	—
Pd/C-K	335.9	337.1	341.2	342.4	70.5	3.89
Pd/C-H	335.8	337.1	341.2	342.4	69.1	3.99

3.3 TEM

To observe the morphology and size of Pd NPs on the prepared Pd/C catalysts, the TEM technique was used and the results were shown in Fig. 3. From Fig. 3(a) (c) (e) (g), the Pd NPs on the prepared Pd/C catalysts were similar and all of them were circular or elliptical particles, suggesting that the morphology of the Pd NPs was not influenced by the Pd precursors. The size of Pd NPs was statistically estimated in Fig. 3(b)(d)(f)(h) and the results indicated that the mean particle sizes of Pd NPs were as follows: Pd/C-A < Pd/C-N < Pd/C-K < Pd/C-H, Pd/C-H, which were 1.7 nm, 2.3 nm, 2.9 nm, and 3.2 nm, respectively. The significant difference in the size of Pd NPs was due to the following reasons. Firstly, among the four selected precursors $Pd(acac)_2$, K_2PdCl_4 and H_2PdCl_4 were coordination compound, and the ligand $[acac]^-$ was significantly larger than the ligand Cl^-. When $Pd(acac)_2$ was used as the precursor, the Pd NPs formed will have larger ligands around them, so it was not easy to migrate to form large Pd grains during the reduction process. Secondly, since the electron mobility was much larger than that of metal ions in plasma, a large number of electrons will migrate to the surface of the catalyst (Di et al. 2018; Liu et al. 2006). Due to a Coulombic interaction electrons will be attracted to cations and repelled by anions. Since the Pd in $Pd(acac)_2$ and $Pd(NO_3)_2$ was a cation, Pd^{2+} will be surrounded by a large number of electrons, which will prevent the migration of Pd NPs. For K_2PdCl_4 and H_2PdCl_4, Pd was located in the anionic $[PdCl_4]^{2-}$ and the electrons will move away from $[PdCl_4]^{2-}$, which was the exact opposite of the cationic Pd precursor. Finally, the kinetic diameters of K^+ and H^+ were 2.66 Å and 10^{-5} Å, and the size of H^+ was almost negligible, which indicates that H_2PdCl_4 was neither protected by electrons nor blocked by any ions in the plasma reduction process, so the largest Pd NPs size was obtained using it as Pd precursor. Correspondingly, we believed that the smaller the particle size of Pd NPs, the better disperse on the support surface. The metal dispersions of the prepared Pd/C catalysts were listed in Table 2. The experimental results were consistent with the expected ones, the metal dispersion and the size of Pd NPs exhibited an inverse relationship in the following order: Pd/C-A > Pd/C-N > Pd/C-K > Pd/C-H. The schematic illustration for the above reduction process was shown in Fig. 4.

3.4 N_2 adsorption-desorption and TG analysis

The results of the N_2 adsorption-desorption characterization of the prepared Pd/C catalysts were shown in Fig. S6 and Table 2. The results showed that the adsorbed amount of N_2 of activated carbon surges in the region of $P/P_0 < 0.1$, and a significant hysteresis loop appears when $P/P_0 > 0.4$, which was due to the capillary coalescence phenomenon. According to the IUPAC classification, the adsorption and desorption isotherm of activated carbon was type IV, indicating that it has both microporous and mesoporous texture (Saka 2012). For the prepared Pd/C catalysts, its N_2 adsorption-desorption isotherm was also type IV, but the adsorbed amount of N_2 showed a significant decrease, which might be caused by the Pd NPs covering the surface of activated carbon and blocking the pores. From Fig. S6(b) and Table 2, it can be seen that the pore size of Pd/C was larger in comparison with that of activated carbon, which may be due to the Pd NPs block the pores with smaller pore size, besides, they accumulate to form large pores. As shown in Table 2, there was almost no difference in the average pore size of the Pd/C, indicating that the type of Pd precursor has no effects on the pore diameter via plasma discharge treatment. However, the Brunauer-Emmett-Teller(BET) specific surface and pore volume of the prepared Pd/C catalysts both

showed varying degrees of decrease compared to activated carbon. This was because the Ar glow plasma was performed at a relatively lower temperature, the residues generated during the reduction process and the Pd precursors that failed to be reduced will be retained in the pore of activated carbon (Wang et al. 2018). The BET specific surface area and pore volume of Pd/C-A, Pd/C-K and Pd/C-H were significantly lower than Pd/C-N, which can be explained by the fact that the Ar plasma can reduce NO_3^- to NO_2 and NO out of activated carbon in addition to reducing Pd^{2+} in $Pd(NO_3)_2{\cdot}2H_2O$, while other Pd precursors will remain on the activated carbon surface in the form of complexes and block the pore, and the reaction process as shown in equations (1)-(8) where H_2O was derived from $Pd(NO_3)_2{\cdot}2H_2O$ and the water adsorbed on the surface of activated carbon. The Pd loadings of Pd/C-N were the highest, about 4.70 wt% closed to the theoretical Pd content of 5 wt% (Table 2) suggesting that activated carbon used has a strong adsorption capacity for $Pd(NO_3)_2$(Zhang et al. 2019). The Pd loadings of Pd/C-K and Pd/C-H were lower than Pd/C-N, and the surface charge distribution of activated carbon was one of the possible reasons for this result. We tested the zeta potential distribution of activated carbon in an aqueous solution, and the results were shown in Figure S5. It can be seen that activated carbon was negatively charged. Due to the Coulomb effect, the activated carbon favors the adsorption of the positive precursor $Pd(NO_3)_2{\cdot}2H_2O$, while on the contrary the negative precursors K_2PdCl_4 and H_2PdCl_4 are not beneficial to be adsorbed by activated carbon(Toebes et al. 2001). the lowest Pd loading of Pd/C-A was due to the bigger and more complicated structure (acetylacetonate complex $Pd(acac)_2$)(Davies et al. 2005).

$e^- + Ar \rightarrow Ar^+ + 2e^-$ (1)

$e^- + Ar \rightarrow Ar^* + e^-$ (2)

$Ar^* + Ar^* \rightarrow Ar^* + Ar + e^-$ (3)

$e^- + H \rightarrow H^+ + 2e^-$ (4)

$e^- + H_2O \rightarrow H^+ + OH + 2e^-$ (5)

$2e^- + Pd^{2+} \rightarrow Pd$ (6)

$NO_3^- + 2H^+ + e^- \rightarrow NO_2\uparrow + H_2O$ (7)

$NO_3^- + 4H^+ + 3e^- \rightarrow NO\uparrow + 2H_2O$ (8)

Table 2
Physical properties of AC and Pd/C catalysts

Samples	BET surface area (m^2/g)	Pore volume (cm^3/g)	Mean pore diameter (nm)	Dispersion (%)[a]	Pd (wt.%)[b]
AC	1263	0.920	2.9	-	-
Pd/C-A	840	0.708	3.4	34	4.49
Pd/C-N	1005	0.801	3.2	20	4.70
Pd/C-K	879	0.724	3.3	14	4.56
Pd/C-H	810	0.668	3.3	12	4.61

[a] From H_2 chemisorption.

[b] Evaluated by TG analysis and the theoretical Pd loading was 5 wt.%.

3.5 Catalytic Dehydrogenation Study

The hydrogen release amounts for H12-NEC on the prepared Pd/C were shown in Fig. 5. It was found that with the extended reaction time, the amount of hydrogen release first increases rapidly and subsequently tends to level off gradually. The catalytic activity of the Pd/C prepared differed greatly, decreasing in the order of Pd/C-A, Pd/C-N, Pd/C-K, and Pd/C-H. The particle size and distribution of Pd as the catalytic activity center of H12-NEC dehydrogenation were closely related to the reaction activity (Wang et al. 2019a). It was found that Pd/C-A with the smallest Pd particle size of 1.7 nm had the highest H_2 evolution, indicating catalytic activity of H12-NEC dehydrogenation was inversely associated with its particle size. From the H12-NEC dehydrogenation results in Table 3, the hydrogen release of Pd/C-A at 1 h was 1.41 wt.% which was 1.56 times of Pd/C-N and 3.61 times of Pd/C-K and Pd/C-H. For Pd/C-H, which had the largest Pd NPs size, the hydrogen release was only 2.37 wt.% after 10 h. In addition, the catalytic activity of the prepared Pd/C catalysts also correlated well with metal dispersion degree, which was positively correlated with H12-NEC dehydrogenation activity (see Table 3), which was in strong agreement with the findings of the H12-NEC dehydrogenation experiment. According to previous results, the presence of inorganic ions such as NO_3^-, Cl^-, and Br^- negatively affects the activity of Pd catalysts (Aramendía et al. 2001; Li et al. 2016; Ukisu et al. 2000; Xia et al. 2009). From the XPS results, it was clear that the residual NO_3^- and Cl^- on the surfaces of Pd/C-N, Pd/C-K and Pd/C-H, which was another reason that affects their catalytic activities. Finally, Pd/C-K and Pd/C-H had smaller BET specific surface area and pore volume across all samples that were not favorable for reactant adsorption and diffusion and thus had lower catalytic activity.

Table 3
H_2 recovery of H12-NEC dehydrogenation over Pd/C catalysts

Catalysts	H_2 recovery in 1 h (wt.%)	Final H_2 recovery after 10 h (wt.%)[a]
Pd/C-A	1.41	5.28
Pd/C-N	0.91	4.91
Pd/C-K	0.39	3.96
Pd/C-H	0.39	2.37

[a] Theoretical H_2 recovery of H12-NEC is 5.79wt.%.

The results of H12-NEC dehydrogenation were shown in Table 4. The catalytic activity of Pd/C-A was the highest at 1 h, which was $4.61*10^{-3}$ $M_{H12-NEC}/(g_{Pd}\cdot s)$, indicating that it could activate more H12-NEC for dehydrogenation at the same time, but its NEC selectivity was the lowest among all catalysts, illustrating that the incomplete dehydrogenation products formed during the dehydrogenation process could be stable on the Pd/C-A catalyst. The catalytic activity of Pd/C-H was slightly higher than that of Pd/C-K, indicating that Pd/C-H can rapidly adsorb and activate H12-NEC to achieve dehydrogenation in the early stage of the reaction. A subsequent kinetic study of the Pd/C catalyst showed that the initial dehydrogenation rate of 4.49 $mM\cdot min^{-1}\cdot g_{cat}^{-1}$ for Pd/C-H was higher than that of 3.55 $mM\cdot min^{-1}\cdot g_{cat}^{-1}$ for Pd/C-K (Table 5), indicating that Pd/C-H can convert more H12-NEC within 1h and thereby its 8H-NEC selectivity (74.0%) was higher than that of Pd/C-K (70.5%). The selectivity of the prepared Pd/C catalysts for 8H-NEC was higher than that of the other two products, which was because 8H-NEC was not easily activated by adsorption on Pd/C catalysts compared with the other products, which was consistent with our previous results (Feng et al. 2020). The specific activity can be used to evaluate the utilization of Pd atoms on Pd/C catalysts. Similarly, the order of specific activity of the prepared Pd/C catalysts was consistent with their order of catalytic activity, where Pd/C-A has the highest specific activity of 4.44 $mol_{NEC}/(mol_{Pd}.min)$, which was 2.5 times higher than that of Pd/C-H. Overall, Pd/C-A has the best performance in catalyzing the dehydrogenation of H12-NEC due to its smallest Pd particle size and highest metal dispersion, as well as the absence of the influence of inorganic ions.

Table 4
The results of H12-NEC dehydrogenation over Pd/C catalysts in 1 h at180℃ and101 KPa

Catalysts	Catalytic activity×10^{-3} (mole $_{H12-NEC}$·gram of Pd^{-1}·s^{-1})	Selectivity (%)			Specific activity (mol_{NEC}/(mol_{Pd}*min))
		8H-NEC	4H-NEC	NEC	
Pd/C-A	4.61	84.1	1.5	14.4	4.44
Pd/C-N	2.78	79.0	2.8	18.2	3.36
Pd/C-K	1.07	70.5	3.1	26.4	1.91
Pd/C-H	1.09	74.0	1.9	24.1	1.78

The distribution of H12-NEC dehydrogenation products was shown in Fig. 6. In addition to the target product NEC, only two incomplete dehydrogenation products appear, octahydro-N-ethylcarbazole (H8-NEC) and tetrahydro-N-ethylcarbazole (H4-NEC), which were consistent with the previously reported literature (Sotoodeh et al. 2009). The distribution of H12-NEC and NEC on all the prepared Pd/C catalysts was the same, the concentration of H12-NEC gradually decreased and the concentration of NEC gradually increased as the reaction time was extended, and the maximum concentration of NEC on Pd/C-A was 3.92 mol/L at the end of the reaction. Due to the low catalytic activity of Pd/C-H, the production rate of H8-NEC and H4-NEC was significantly higher than the consumption rate, and the concentration sustained to increase, however, did not decrease within 600 min. In general, the precursors had no effect on the species of H12-NEC dehydrogenation intermediates over Pd/C catalysts, and the dehydrogenation pathways can be considered as H12-NEC→H8-NEC→H4-NEC→NEC, which was in keeping with previously reported literature (Yang et al. 2014). There were large differences in the dehydrogenation activity of the prepared Pd/C catalysts, which can adsorption and activation capacity of the intermediates. Compared with the other catalysts, Pd/C-A with the highest catalytic activity was able to convert more H12-NEC and consume the generated H8-NEC and H4-NEC in a shorter period of time.

It has been shown that the dehydrogenation of H12-NEC obeys the rules of the first-order kinetic reaction, which can be seen by Eq. (9)(10), with time as abscissa and Ln($C_{H12-NEC/C0}$) as ordinate to make a graph, and the slope of the line obtained after a linear fit was rate constant (Sotoodeh et al. 2009). Initial dehydrogenation rates of H12-NEC dehydrogenation were calculated via Eq. (11), where $C_{H12-NEC}$ and C_0 were the concentration and initial concentration corresponding to H12-NEC at time t, respectively, k was the rate constant, t was the reaction time, and $m_{catalyst}$ was the mass of the catalyst. The results of the kinetic study were shown in Fig. 7 and Table 5.

$$r = \frac{dC_{H12\text{-}NEC}}{dt} = -kC_{H12\text{-}NEC} \quad (9)$$

$$\ln\left(\frac{C_{H12\text{-}NEC}}{C_0}\right) = -kt \quad (10)$$

$$\text{Initial rate} = \frac{k \times C_0}{m_{catalyst}} \quad (11)$$

The R^2 values fitted by the selected catalysts dehydrogenation results all reached 98%, indicating that the fitted equations are very linear between t and Ln($C_{H12-NEC}/C_0$), demonstrating that H12-NEC dehydrogenation was a Pseudo-first-order reaction. Pd/C-A had the largest k value of 0.0074 min^{-1} and the highest initial reaction rate of 10.53 $Mm \cdot min^{-1} \cdot g_{cat}^{-1}$ than other Pd/C catalysts. This was mainly because it has the highest catalytic activity and the strongest adsorption and activation capacity for H12-NEC. The initial dehydrogenation activities of the prepared Pd/C were ranked as follows: Pd/C-A > Pd/C-N > Pd/C-H > Pd/C-K. Due to the different physicochemical properties, the precursors significantly affect the kinetic process of H12-NEC dehydrogenation over Pd/C catalysts. Therefore, we investigated the kinetic characteristics of H12-NEC dehydrogenation at different reaction temperatures and calculated their apparent activation energies using the Arrhenius equation.

Table 5
The kinetic results of H12-NEC dehydrogenation over Pd/C catalysts

Catalysts	Rate constant, [a] k (min^{-1})	R^2	Initial rate ($mM \cdot min^{-1} \cdot g_{cat}^{-1}$)
Pd/C-A	0.0074	0.9955	10.53
Pd/C-N	0.0067	0.9800	9.48
Pd/C-K	0.0025	0.9806	3.55
Pd/C-H	0.0032	0.9829	4.49

[a] First-order rate constant for H12-NEC consumption.

To ensure that the Pd/C catalyst also has high activity for the reaction at 160°C and reduce the experimental error, the amount of catalyst was increased to adjust the Pd/H12-NEC (molar ratio) was adjusted from 0.03–0.2% when calculating the k value of the H12-NEC dehydrogenation reaction at different temperatures. Similarly, a linear fit was performed to calculate the k for the reaction results of Pd/C catalysts at different temperatures, and the results of the fit were shown in Fig. S7 and Table S1. The R^2 was given in parenthesis. The fit results of H12-NEC dehydrogenation also showed good linearity after increasing the catalyst dosage. At the same temperature, the rate constant of Pd/C-A was still the largest, which was attributed to its high activity. The apparent activation energy of Pd/C catalysts was obtained from the slopes of the lines fitted in Fig. S8, and the results were listed in Table S1. Combined

with the previous discussion, it was clear that the catalytic performance of Pd/C-A was significantly better than that of Pd/C-N, and we predicted that the apparent activation energy of Pd/C-N would be higher than that of Pd/C-A, but the results did not match the prediction, and they were basically the same, 77 KJ/mol and 76 KJ/mol, respectively. This was probably because the BET specific surface area and pore volume and Pd content of Pd/C-N were significantly higher than those of Pd/C-A. The larger specific surface area and pore volume were favorable for the adsorption of reactants, the high Pd reduction degree and content means that it has more active Pd species, these compensate to some extent the performance gap of Pd/C-N due to the difference in Pd particle size, while eliminating part of the negative effects caused by NO_3^-.

4. Conclusion

In summary, we prepared Pd/C catalysts via Ar glow-discharge plasma reduction, using activated carbon as the support and $Pd(acac)_2$, $Pd(NO_3)_2$, K_2PdCl_4 and H_2PdCl_4 as the Pd precursors. The physicochemical properties of the prepared Pd/C catalysts were analyzed by comprehensive characterization. It was found that the Pd/C-A has the smallest Pd particle size of 1.7 nm and the highest dispersion of 34%. The H12-NEC dehydrogenation results showed that the Pd precursors had a strong influence on the catalytic activity of the prepared Pd/C catalysts. The catalytic activities were arranged in the following order of Pd/C-A□Pd/C-N□Pd/C-K□Pd/C-H. Pd/C-A showed the best catalytic performance with a specific activity of 4.44 $mol_{NEC}/(mol_{Pd}*min)$, which was 2.5 times higher than that of Pd/C-H. This was attributed to a larger ligand of $Pd(acac)_2$, and Pd NPs were not easy to agglomerate after in situ reduction of plasma. Meanwhile, in Ar Plasma, the electron mobility was much greater than that of heavy ions, for cationic Pd precursors electrons will be attracted around Pd^{2+} via Coulomb interaction, which further prevents the growth of Pd particles. The reaction barrier for dehydrogenation of 12H-NEC over the prepared Pd/C catalyst was calculated to obtain the apparent activation energy in the order of Pd/C-A (76 KJ/mol) ≈ Pd/C-N (77 KJ/mol) < Pd/C-K (114 KJ/mol) < Pd/C-H (143 KJ/ mol). The present work provides a reference for us and our colleagues in the selection of Pd precursors for further design of Pd/C catalysts using Ar glow discharge plasma.

Declarations

Ethics approval and consent to participate

Not applicable.

Consent for publication

Not applicable.

Availability of data and materials

The datasets used and analyzed during the current study are available from the corresponding author on reasonable request.

Competing interests

The authors declare that they have no competing interests.

All authors certify that they have no affiliations with or involvement in any organization or entity with any financial interest or non-financial interest in the subject matter or materials discussed in this manuscript.

Funding

This work was supported by the National Key R&D Program(2018YFE0108800), the National Natural Science Foundation of China (21676074) and the Science Foundation of Heilongjiang Academy of Sciences (KY2020SH01).

Authors' contributions

All authors contributed to the study conception and design. Material preparation, data collection and analysis were performed by Zhaolu Feng, Xiaomin Chen and Xuefeng Bai. The first draft of the manuscript was written by Zhaolu Feng and all authors commented on previous versions of the manuscript. All authors read and approved the final manuscript.

Conceptualization: Xuefeng Bai and Zhaolu Feng; Methodology: Zhaolu Feng; Formal analysis and investigation: Zhaolu Feng; Writing - original draft preparation: Zhaolu Feng; Writing - review and editing: Xuefeng Bai; Funding acquisition: Xuefeng Bai; Resources: Xuefeng Bai; Supervision: Xuefeng Bai and Xiaomin Chen.

Acknowledgments

This work was supported by the National Key R&D Program(2018YFE0108800), the National Natural Science Foundation of China (21676074) and the Science Foundation of Heilongjiang Academy of Sciences (KY2020SH01).

References

Aakko-Saksa PT, Cook C, Kiviaho J, Repo T (2018) Liquid organic hydrogen carriers for transportation and storing of renewable energy – Review and discussion. Journal of Power Sources 396:803-823. https://doi.org/10.1016/j.jpowsour.2018.04.011

Amende M et al. (2014a) Size and Structure Effects Controlling the Stability of the Liquid Organic Hydrogen Carrier Dodecahydro-N-ethylcarbazole during Dehydrogenation over Pt Model Catalysts. The Journal of Physical Chemistry Letters 5:1498-1504. https://doi.org/10.1021/jz500157r

Amende M et al. (2014b) Model Catalytic Studies of Liquid Organic Hydrogen Carriers: Dehydrogenation and Decomposition Mechanisms of Dodecahydro-N-ethylcarbazole on Pt(111). ACS Catalysis 4:657-665. https://doi.org/10.1021/cs400946x

Aramendía MA, Benítez JA, Boráu V, Jiménez C, Marinas JM, Moreno A (1997) Dehydrogenation of cyclohexane over Pt/SiO_2–$AlPO_4$ catalysts, I. Influence of the catalyst particle size. Reaction Kinetics and Catalysis Letters 62:23-31. https://doi.org/10.1007/BF02475709

Aramendía MA, Burch R, García IM, Marinas A, Marinas JM, Southward BWL, Urbano FJ (2001) The effect of the addition of sodium compounds in the liquid-phase hydrodechlorination of chlorobenzene over palladium catalysts. Applied Catalysis B: Environmental 31:163-171. https://doi.org/10.1016/S0926-3373(00)00280-0

Baylet A, Royer S, Marécot P, Tatibouët JM, Duprez D (2008) Effect of Pd precursor salt on the activity and stability of Pd-doped hexaaluminate catalysts for the CH_4 catalytic combustion. Applied Catalysis B: Environmental 81:88-96. https://doi.org/10.1016/j.apcatb.2007.12.004

Crabtree RH (2017) Nitrogen-Containing Liquid Organic Hydrogen Carriers: Progress and Prospects. ACS Sustainable Chemistry & Engineering 5:4491-4498. https://doi.org/10.1021/acssuschemeng.7b00983

Cui Y, Kwok S, Bucholtz A, Davis B, Whitney RA, Jessop PG (2008) The effect of substitution on the utility of piperidines and octahydroindoles for reversible hydrogen storage. New Journal of Chemistry 32:1027-1037. https://doi.org/10.1039/B718209K

Das D, Veziroğlu TN (2001) Hydrogen production by biological processes: a survey of literature. International Journal of Hydrogen Energy 26:13-28. https://doi.org/10.1016/S0360-3199(00)00058-6

Davies D, Donald S, Macgregor S (2005) Computational Study of the Mechanism of Cyclometalation by Palladium Acetate. Journal of the American Chemical Society 127:13754-13755. https://doi.org/10.1021/ja052047w

Deng J-F, Li H, Wang W (1999) Progress in design of new amorphous alloy catalysts. Catalysis Today 51:113-125. https://doi.org/10.1016/S0920-5861(99)00013-9

Di L, Zhang J, Ma C, Tu X, Zhang X (2019) Atmospheric-pressure dielectric barrier discharge cold plasma for synthesizing high performance Pd/C formic acid dehydrogenation catalyst. Catalysis Today 337:201-207. https://doi.org/10.1016/j.cattod.2019.02.062

Di L, Zhang J, Zhang X (2018) A review on the recent progress, challenges, and perspectives of atmospheric-pressure cold plasma for preparation of supported metal catalysts. Plasma Processes and Polymers 15:1700234. https://doi.org/10.1002/ppap.201700234

Eblagon KM, Rentsch D, Friedrichs O, Remhof A, Zuettel A, Ramirez-Cuesta AJ, Tsang SC (2010) Hydrogenation of 9-ethylcarbazole as a prototype of a liquid hydrogen carrier. International Journal of Hydrogen Energy 35:11609-11621. https://doi.org/10.1016/j.ijhydene.2010.03.068

Eblagon KM, Tam K, Yu KMK, Tsang SCE (2012) Comparative Study of Catalytic Hydrogenation of 9-Ethylcarbazole for Hydrogen Storage over Noble Metal Surfaces. The Journal of Physical Chemistry C 116:7421-7429. https://doi.org/10.1021/jp212249g

Fei S, Han B, Li L, Mei P, Zhu T, Yang M, Cheng H (2017) A study on the catalytic hydrogenation of N-ethylcarbazole on the mesoporous Pd/MoO3 catalyst. International Journal of Hydrogen Energy 42:25942-25950. https://doi.org/10.1016/j.ijhydene.2017.08.204

Feng Z, Chen X, Bai X (2020) Catalytic dehydrogenation of liquid organic hydrogen carrier dodecahydro-N-ethylcarbazole over palladium catalysts supported on different supports. Environmental Science and Pollution Research 27:36172-36185. https://doi.org/10.1007/s11356-020-09698-w

Gianotti E, Taillades-Jacquin M, Rozière J, Jones DJ (2018) High-Purity Hydrogen Generation via Dehydrogenation of Organic Carriers: A Review on the Catalytic Process. ACS Catalysis 8:4660-4680. https://doi.org/10.1021/acscatal.7b04278

He T, Pachfule P, Wu H, Xu Q, Chen P (2016) Hydrogen carriers. Nature Reviews Materials 1:16059. https://doi.org/10.1038/natrevmats.2016.59

Hodoshima S, Arai H, Takaiwa S, Saito Y (2003) Catalytic decalin dehydrogenation/naphthalene hydrogenation pair as a hydrogen source for fuel-cell vehicle. International Journal of Hydrogen Energy 28:1255-1262. https://doi.org/10.1016/S0360-3199(02)00250-1

Holladay JD, Hu J, King DL, Wang Y (2009) An overview of hydrogen production technologies. Catalysis Today 139:244-260. https://doi.org/10.1016/j.cattod.2008.08.039

Kim K, Oh J, Kim TW, Park JH, Han JW, Suh Y-W (2017) Different catalytic behaviors of Pd and Pt metals in decalin dehydrogenation to naphthalene. Catalysis Science & Technology 7:3728-3735. https://doi.org/10.1039/C7CY00569E

Kim Y, Kim DH (2019) Understanding the effect of Pd size on formic acid dehydrogenation via size-controlled Pd/C catalysts prepared by $NaBH_4$ treatment. Applied Catalysis B: Environmental 244:684-693. https://doi.org/10.1016/j.apcatb.2018.12.008

Kim Y, Song Y, Choi Y, Jeong K, Park JH, Ko KC, Na K (2021) Catalytic Consequences of Supported Pd Catalysts on Dehydrogenative H_2 Evolution from 2-[(n-Methylcyclohexyl)methyl]piperidine as the Liquid Organic Hydrogen Carrier. ACS Sustainable Chemistry & Engineering 9:809-821. https://doi.org/10.1021/acssuschemeng.0c07338

Kinnunen NM, Suvanto M, Moreno MA, Savimäki A, Kallinen K, Kinnunen TJJ, Pakkanen TA (2009) Methane oxidation on alumina supported palladium catalysts: Effect of Pd precursor and solvent. Applied Catalysis A: General 370:78-87. https://doi.org/10.1016/j.apcata.2009.09.018

Li B, Li H, Weng W-Z, Zhang Q, Huang C-J, Wan H-L (2013) Synthesis gas production from partial oxidation of methane over highly dispersed Pd/SiO_2 catalyst. Fuel 103:1032-1038. https://doi.org/10.1016/j.fuel.2012.09.059

Li X, Guo Z, Xiao C, Goh TW, Tesfagaber D, Huang W (2014) Tandem Catalysis by Palladium Nanoclusters Encapsulated in Metal–Organic Frameworks. ACS Catalysis 4:3490-3497. https://doi.org/10.1021/cs5006635

Li Y, Liu H, Ma L, He D (2016) Influence of Pd precursors and Cl addition on performance of Pd-Re catalysts in glycerol hydrogenolysis to propanediols. Applied Catalysis A: General 522:13-20. https://doi.org/10.1016/j.apcata.2016.04.029

Liu C-J, Zhao Y, Li Y, Zhang D-S, Chang Z, Bu X-H (2014) Perspectives on Electron-Assisted Reduction for Preparation of Highly Dispersed Noble Metal Catalysts. ACS Sustainable Chemistry & Engineering 2:3-13. https://doi.org/10.1021/sc400376m

Liu C-j et al. (2006) Plasma application for more environmentally friendly catalyst preparation. Pure and Applied Chemistry 78:1227-1238. https://doi.org/10.1351/pac200678061227

Liu T, Cui Z, Liu Y, Bai X (2019) In-situ fabrication of ultrafine Pd supported on nitrogen-doped reduced graphene oxide via nitrogen glow discharge plasma for catalytic reduction of 4-Nitrophenol. Applied Catalysis A: General 588:117278. https://doi.org/10.1016/j.apcata.2019.117278

Liu Y, Bai X (2016) Preparation of Pd Nanoparticles Supported on Activated Carbon via Glow Discharge Plasma and Their Catalytic Properties for Suzuki Coupling Reactions. Chemistry Letters 45:705-707. https://doi.org/10.1246/cl.160219

Liu Y, Bai X, Li S (2018) In-situ preparation of Pd nanoparticles in the pore channel of CMK-3 for Suzuki coupling reaction. Microporous and Mesoporous Materials 260:40-44. https://doi.org/10.1016/j.micromeso.2017.06.006

Makowski P, Thomas A, Kuhn P, Goettmann F (2009) Organic materials for hydrogen storage applications: From physisorption on organic solids to chemisorption in organic molecules. Energy & Environmental Science - ENERGY ENVIRON SCI 2. https://doi.org/10.1039/b822279g

Mallick K, Witcomb MJ, Scurrell MS (2004) Supported gold catalysts prepared by in situ reduction technique: preparation, characterization and catalytic activity measurements. Applied Catalysis A: General 259:163-168. https://doi.org/10.1016/j.apcata.2003.09.043

Modisha PM, Ouma CNM, Garidzirai R, Wasserscheid P, Bessarabov D (2019) The Prospect of Hydrogen Storage Using Liquid Organic Hydrogen Carriers. Energy & Fuels 33:2778-2796. https://doi.org/10.1021/acs.energyfuels.9b00296

Moradi R, Groth KM (2019) Hydrogen storage and delivery: Review of the state of the art technologies and risk and reliability analysis. International Journal of Hydrogen Energy 44:12254-12269. https://doi.org/10.1016/j.ijhydene.2019.03.041

Oh J, Kim TW, Jeong K, Park JH, Suh Y-W (2018) Enhanced Activity and Stability of a Carbon-Coated Alumina-Supported Pd Catalyst in the Dehydrogenation of a Liquid Organic Hydrogen Carrier, Perhydro 2-(n-methylbenzyl)Pyridine. ChemCatChem 10:3892-3900 https://doi.org/10.1002/cctc.201800537

Panpranot J, Tangjitwattakorn O, Praserthdam P, Goodwin JG (2005) Effects of Pd precursors on the catalytic activity and deactivation of silica-supported Pd catalysts in liquid phase hydrogenation. Applied Catalysis A: General 292:322-327. https://doi.org/10.1016/j.apcata.2005.06.008

Papp C, Wasserscheid P, Libuda J, Steinrück H-P (2014) Liquid Organic Hydrogen Carriers: Surface Science Studies of Carbazole Derivatives. The Chemical Record 14:879-896. https://doi.org/10.1002/tcr.201402014

Peters W, Seidel A, Herzog S, Bösmann A, Schwieger W, Wasserscheid P (2015) Macrokinetic effects in perhydro-N-ethylcarbazole dehydrogenation and H_2 productivity optimization by using egg-shell catalysts. Energy & Environmental Science 8:3013-3021. https://doi.org/10.1039/C5EE02024G

Preuster P, Papp C, Wasserscheid P (2017) Liquid Organic Hydrogen Carriers (LOHCs): Toward a Hydrogen-free Hydrogen Economy. Accounts of Chemical Research 50:74-85. https://doi.org/10.1021/acs.accounts.6b00474

Rotunno F et al. (2006) Preparation of Pd/C catalysts: from the Pd-precursor solution to the final systems. In: Gaigneaux EM, Devillers M, De Vos DE, Hermans S, Jacobs PA, Martens JA, Ruiz P (eds) Studies in Surface Science and Catalysis, vol 162. Elsevier, pp 721-728.

Saka C (2012) BET, TG–DTG, FT-IR, SEM, iodine number analysis and preparation of activated carbon from acorn shell by chemical activation with $ZnCl_2$. Journal of Analytical and Applied Pyrolysis 95:21-24. https://doi.org/10.1016/j.jaap.2011.12.020

Satyapal S, Petrovic J, Read C, Thomas G, Ordaz G (2007) The U.S. Department of Energy's National Hydrogen Storage Project: Progress towards meeting hydrogen-powered vehicle requirements. Catalysis Today 120:246-256. https://doi.org/10.1016/j.cattod.2006.09.022

Schmidt F (2001) New catalyst preparation technologies—observed from an industrial viewpoint. Applied Catalysis A: General 221:15-21. https://doi.org/10.1016/S0926-860X(01)00802-X

Scirè S, Minicò S, Crisafulli C (2002) Selective hydrogenation of phenol to cyclohexanone over supported Pd and Pd-Ca catalysts: an investigation on the influence of different supports and Pd precursors. Applied Catalysis A: General 235:21-31. https://doi.org/10.1016/S0926-860X(02)00237-5

Sobota M et al. (2011) Dehydrogenation of Dodecahydro-N-ethylcarbazole on Pd/Al_2O_3 Model Catalysts. Chemistry – A European Journal 17:11542-11552 https://doi.org/10.1002/chem.201101311

Sotoodeh F, Huber BJM, Smith KJ (2012) Dehydrogenation kinetics and catalysis of organic heteroaromatics for hydrogen storage. International Journal of Hydrogen Energy 37:2715-2722. https://doi.org/10.1016/j.ijhydene.2011.03.055

Sotoodeh F, Smith KJ (2013) An overview of the kinetics and catalysis of hydrogen storage on organic liquids. The Canadian Journal of Chemical Engineering 91:1477-1490 https://doi.org/10.1002/cjce.21871

Sotoodeh F, Zhao L, Smith KJ (2009) Kinetics of H_2 recovery from dodecahydro-N-ethylcarbazole over a supported Pd catalyst. Applied Catalysis A: General 362:155-162. https://doi.org/10.1016/j.apcata.2009.04.039

Stark K, Emel'yanenko VN, Zhabina AA, Varfolomeev MA, Verevkin SP, Müller K, Arlt W (2015) Liquid Organic Hydrogen Carriers: Thermophysical and Thermochemical Studies of Carbazole Partly and Fully Hydrogenated Derivatives. Industrial & Engineering Chemistry Research 54:7953-7966. https://doi.org/10.1021/acs.iecr.5b01841

Tarasov AL, Tkachenko OP, Kustov LM (2018) Mono and Bimetallic Pt–(M)/Al_2O_3 Catalysts for Dehydrogenation of Perhydro-N-ethylcarbazole as the Second Stage of Hydrogen Storage. Catalysis Letters 148:1472-1477. https://doi.org/10.1007/s10562-018-2325-4

Toebes ML, van Dillen JA, de Jong KP (2001) Synthesis of supported palladium catalysts. Journal of Molecular Catalysis A: Chemical 173:75-98. https://doi.org/10.1016/S1381-1169(01)00146-7

Ukisu Y, Kameoka S, Miyadera T (2000) Catalytic dechlorination of aromatic chlorides with noble-metal catalysts under mild conditions: approach to practical use. Applied Catalysis B: Environmental 27:97-104. https://doi.org/10.1016/S0926-3373(00)00137-5

Veziroğlu TN, Şahi˙n S (2008) 21st Century's energy: Hydrogen energy system. Energy Conversion and Management 49:1820-1831. https://doi.org/10.1016/j.enconman.2007.08.015

Wang B, Chang T-y, Jiang Z, Wei J-j, Fang T (2019a) Component controlled synthesis of bimetallic PdCu nanoparticles supported on reduced graphene oxide for dehydrogenation of dodecahydro-N-ethylcarbazole. Applied Catalysis B: Environmental 251:261-272. https://doi.org/10.1016/j.apcatb.2019.03.071

Wang B et al. (2020) Facet-dependent catalytic activities of Pd/rGO: Exploring dehydrogenation mechanism of dodecahydro-N-ethylcarbazole. Applied Catalysis B: Environmental 266:118658. https://doi.org/10.1016/j.apcatb.2020.118658

Wang B, Yan T, Chang T, Wei J, Zhou Q, Yang S, Fang T (2017) Palladium supported on reduced graphene oxide as a high-performance catalyst for the dehydrogenation of dodecahydro-N-ethylcarbazole. Carbon 122:9-18. https://doi.org/10.1016/j.carbon.2017.06.021

Wang S, Huang H, Bruneau C, Fischmeister C (2019) Iridium-Catalyzed Hydrogenation and Dehydrogenation of N-Heterocycles in Water under Mild Conditions. ChemSusChem 12:2350-2354. https://doi.org/10.1002/cssc.201900626

Wang Y et al. (2015) Effect of metal precursors on the performance of Pt/ZSM-22 catalysts for n-hexadecane hydroisomerization. Journal of Catalysis 322:1-13. https://doi.org/10.1016/j.jcat.2014.11.004

Wang Z, Tonks I, Belli J, Jensen CM (2009) Dehydrogenation of N-ethyl perhydrocarbazole catalyzed by PCP pincer iridium complexes: Evaluation of a homogenous hydrogen storage system. Journal of Organometallic Chemistry 694:2854-2857. https://doi.org/10.1016/j.jorganchem.2009.03.052

Wang Z, Zhang Y, Neyts EC, Cao X, Zhang X, Jang BWL, Liu C-j (2018) Catalyst Preparation with Plasmas: How Does It Work?. ACS Catalysis 8:2093-2110. https://doi.org/10.1021/acscatal.7b03723

Wulf C, Zapp P (2018) Assessment of system variations for hydrogen transport by liquid organic hydrogen carriers. International Journal of Hydrogen Energy 43:11884-11895. https://doi.org/10.1016/j.ijhydene.2018.01.198

Xia C et al. (2009) The influence of ion effects on the Pd-catalyzed hydrodechlorination of 4-chlorophenol in aqueous solutions. Catalysis Communications 10:1443-1445. https://doi.org/10.1016/j.catcom.2009.03.018

Xie Y-h et al. (2015) Mechanistic aspects of formation of sintering-resistant palladium nanoparticles over SiO2 prepared using Pd(acac)2 as precursor. Applied Catalysis A: General 504:179-186. https://doi.org/10.1016/j.apcata.2014.12.008

Xie Y, Milstein D (2019) Pd Catalyzed, Acid Accelerated, Rechargeable, Liquid Organic Hydrogen Carrier System Based on Methylpyridines/Methylpiperidines. ACS Applied Energy Materials 2:4302-4308. https://doi.org/10.1021/acsaem.9b00523

Xu W, Zhan Z, Di L, Zhang X (2015) Enhanced activity for CO oxidation over Pd/Al2O3 catalysts prepared by atmospheric-pressure cold plasma. Catalysis Today 256:148-152. https://doi.org/10.1016/j.cattod.2015.01.017

Yang M, Dong Y, Fei S, Ke H, Cheng H (2014) A comparative study of catalytic dehydrogenation of perhydro-N-ethylcarbazole over noble metal catalysts. International Journal of Hydrogen Energy 39:18976-18983. https://doi.org/10.1016/j.ijhydene.2014.09.123

Yang M, Han C, Ni G, Wu J, Cheng H (2012) Temperature controlled three-stage catalytic dehydrogenation and cycle performance of perhydro-9-ethylcarbazole. International Journal of Hydrogen Energy 37:12839-12845. https://doi.org/10.1016/j.ijhydene.2012.05.092

Yoshii K, Oshino Y, Tachikawa N, Toshima K, Katayama Y (2015) Electrodeposition of palladium from palladium(II) acetylacetonate in an amide-type ionic liquid. Electrochemistry Communications 52:21-24. https://doi.org/10.1016/j.elecom.2015.01.003

Zhang F, Zhao P, Niu M, Maddy J (2016) The survey of key technologies in hydrogen energy storage. International Journal of Hydrogen Energy 41:14535-14552. https://doi.org/10.1016/j.ijhydene.2016.05.293

Zhang J, Di L, Yu F, Duan D, Zhang X (2018) Atmospheric-Pressure Cold Plasma Activating Au/P25 for CO Oxidation: Effect of Working Gas. Nanomaterials 8:742. https://doi.org/10.3390/nano8090742

Zhang J, Wang H, Zhao Q, Di L, Zhang X (2020) Facile synthesis of PdAu/C by cold plasma for efficient dehydrogenation of formic acid. International Journal of Hydrogen Energy 45:9624-9634. https://doi.org/10.1016/j.ijhydene.2020.01.196

Zhang X, Du Y, Jiang H, Liu Y, Chen R (2019) Matching Relationship Between Carbon Material and Pd Precursor. Catalysis Letters 149:813-822. https://doi.org/10.1007/s10562-018-2630-y

Zhu M, Xu L, Du L, An Y, Wan C (2018) Palladium Supported on Carbon Nanotubes as a High-Performance Catalyst for the Dehydrogenation of Dodecahydro-N-ethylcarbazole. Catalysts 8:638. https://doi.org/10.3390/catal8120638

Zou J-J, Zhang Y-p, Liu C-J (2006) Reduction of Supported Noble-Metal Ions Using Glow Discharge Plasma Langmuir 22:11388-11394. https://doi.org/10.1021/la061795b

Figures

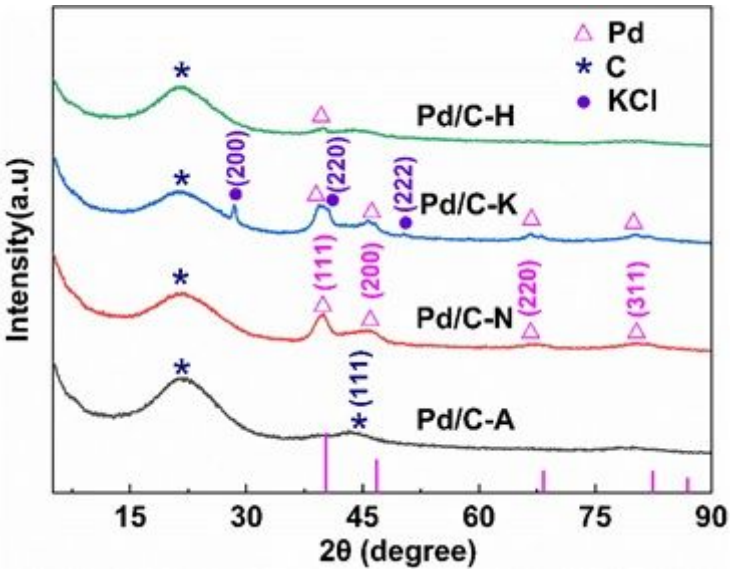

Figure 1

XRD patterns of Pd/C catalysts

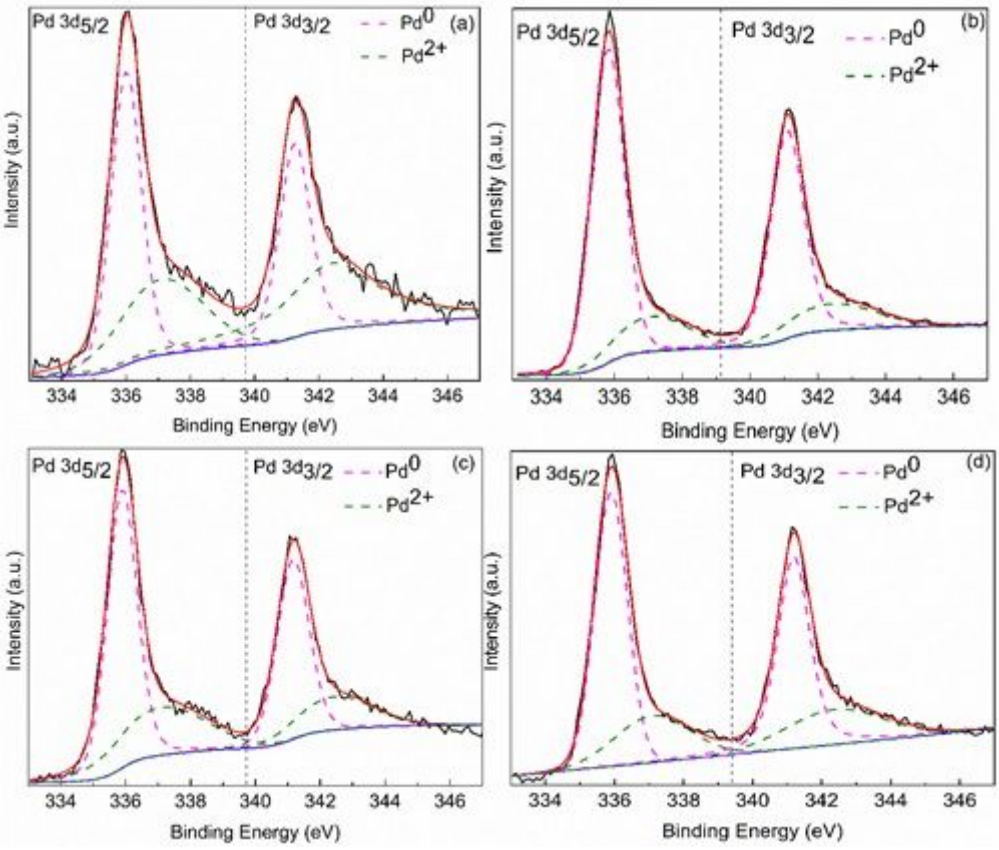

Figure 2

XPS spectra of Pd 3d in Pd/C catalysts (a)Pd/C-A (b) Pd/C-N (c)Pd/C-K (d) Pd/C-H

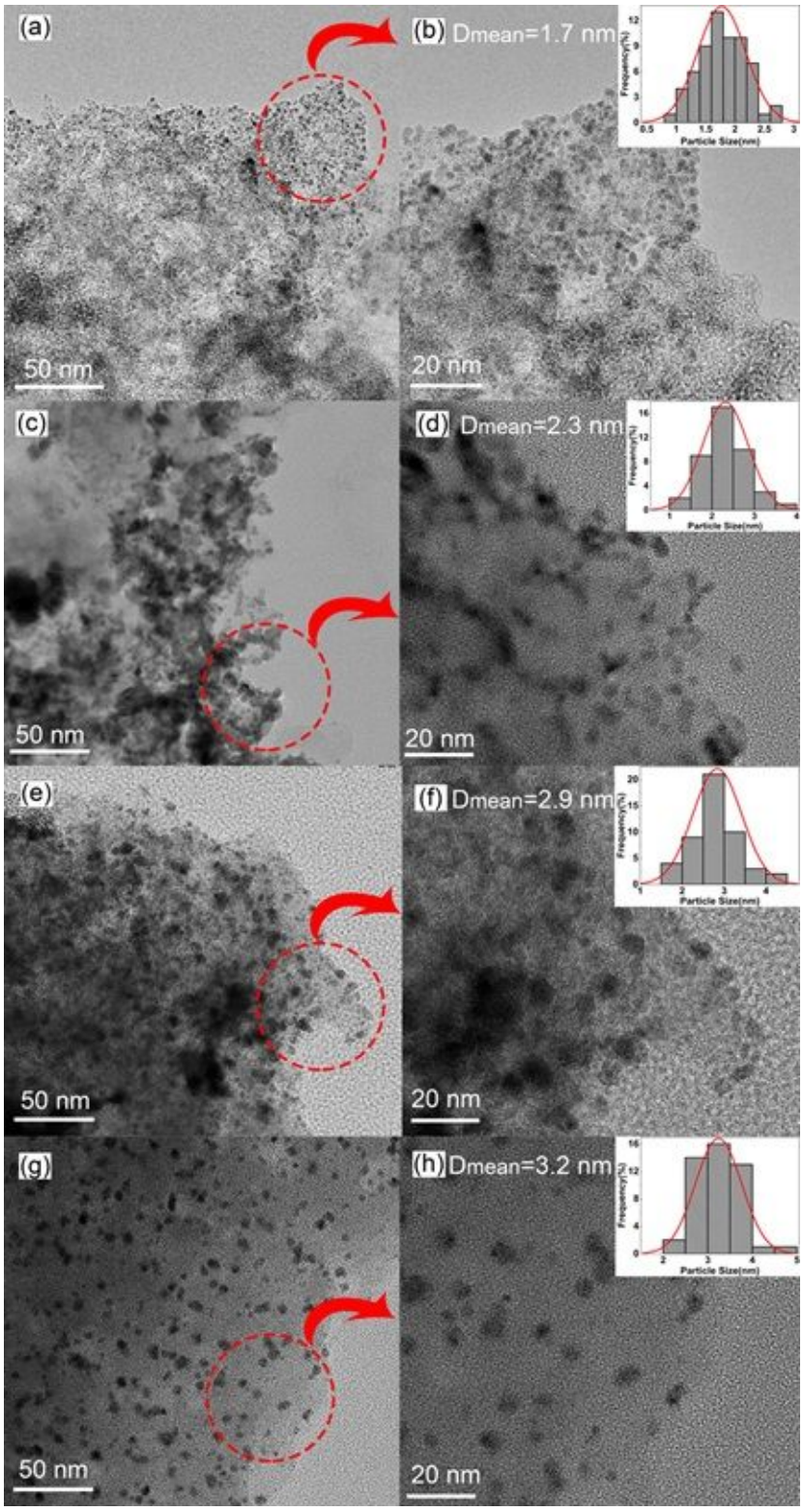

Figure 3

TEM image and NPs size histogram inset of Pd/C catalysts (a,b)Pd/C-A (c,d) Pd/C-N (e,f)Pd/C-K (g,h) Pd/C-H

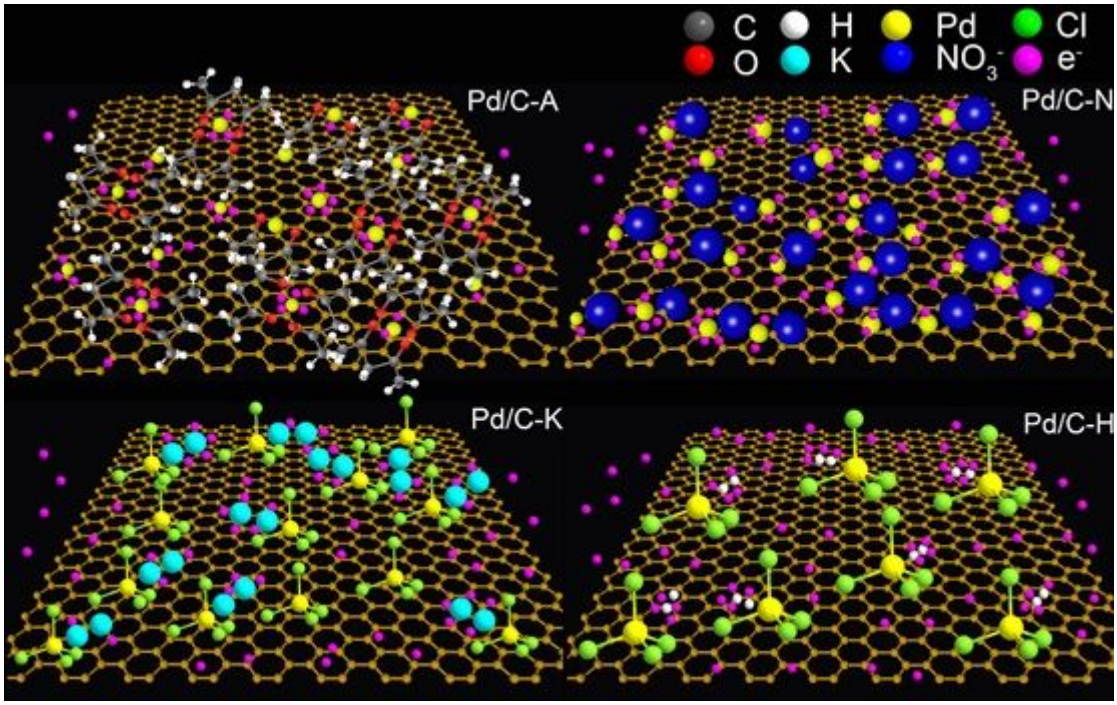

Figure 4

Schematic illustration of Pd/C catalysts

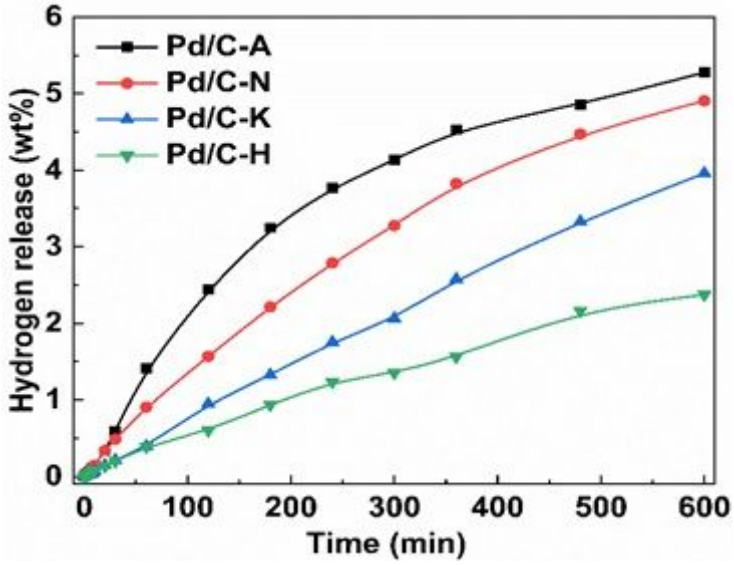

Figure 5

Hydrogen release curves for H12-NEC dehydrogenation at 180℃ and 101 kPa over Pd/C catalysts

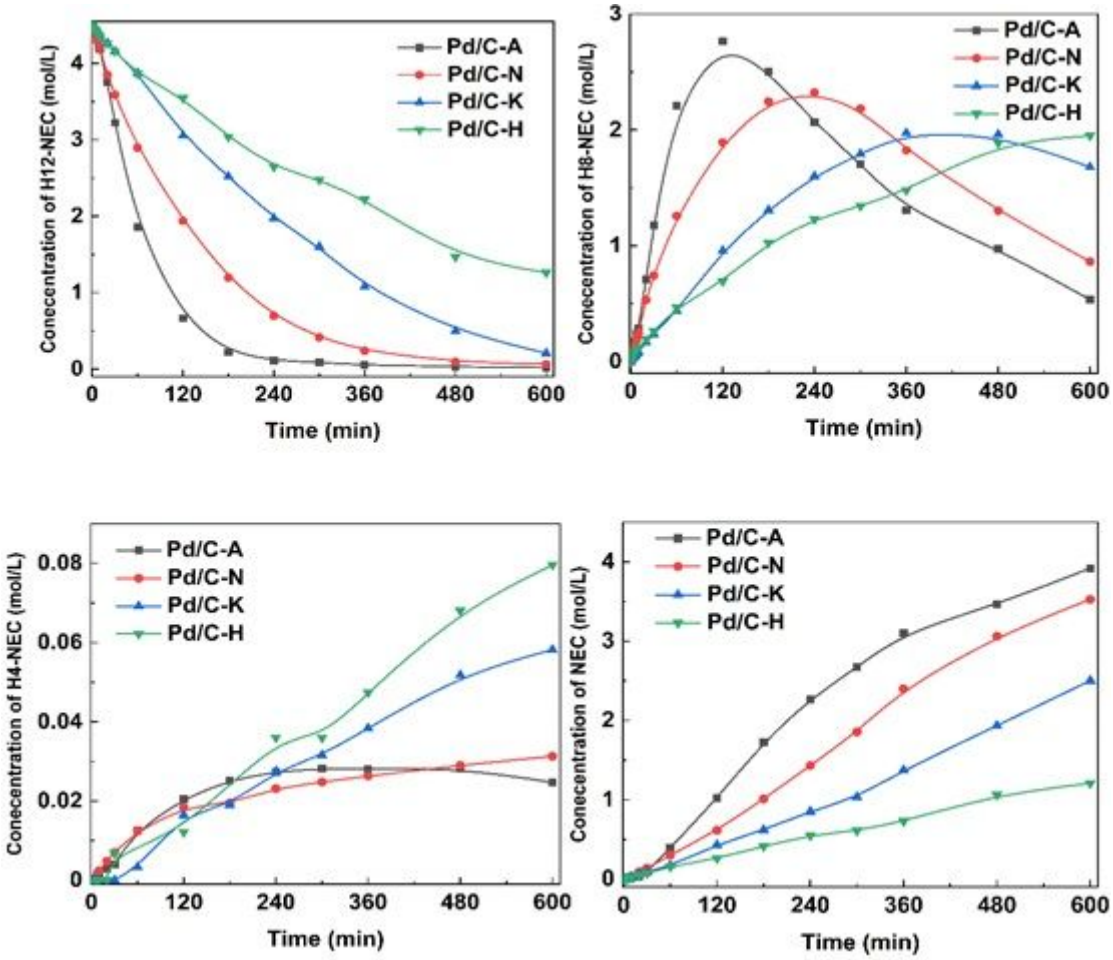

Figure 6

Product distributions of 12H-NEC dehydrogenation over Pd/C catalysts at 180 ℃ and 101 kPa

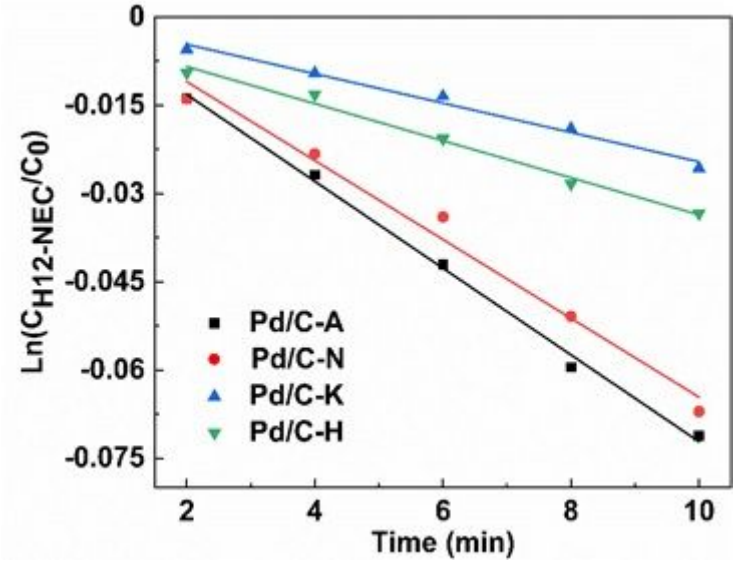

Figure 7

The kinetics of H12-NEC dehydrogenation over Pd/C catalyst at 180 ℃ and 101 kPa

Supplementary Files

This is a list of supplementary files associated with this preprint. Click to download.

- Supplementarymaterial.docx